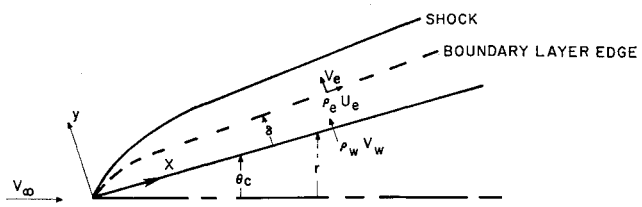

Fig. 1 Flow field about a cone.

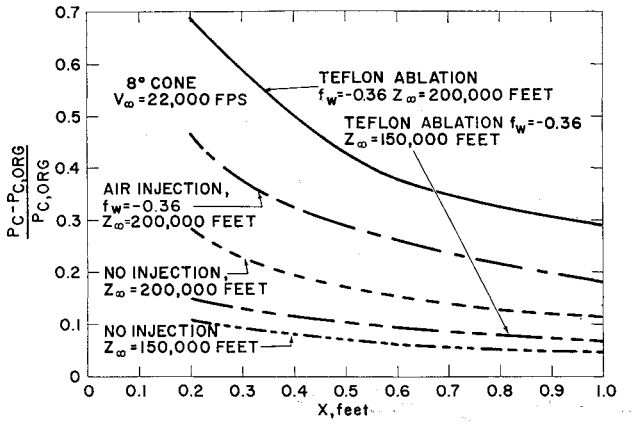

Fig. 2 Induced cone pressure.

where

$$\delta^* = \int_0^\infty \left(1 - \frac{\rho u}{\rho_e U_e}\right) dy$$

The foregoing expression for V_e/U_e may be simplified by employing the following assumptions. 1) $\delta \approx \delta^*$; and 2) $r \gg \delta$ (neglecting transverse curvature). Then

$$V_e/U_e = (\rho_w V_w/\rho_e U_e) + (d\delta^*/dx)$$

Mann[2] has derived the analogous expression for two-dimensional flow. The effective body shape or local cone angle then becomes

$$\theta_{\text{eff}} = \theta_{c,\text{org}} + (\rho_w V_w/\rho_e U_e) + (d\delta^*/dx)$$

The quantities $\rho_w V_w/\rho_e U_e$ and $d\delta^*/dx$ are obtained from the solution of the similar boundary-layer equations[3] wherein the gaseous composition of the boundary layer is assumed to be a binary mixture of equilibrium air and injected gas.

By using the noninteracting or original conical flow, the effective body shape may then be rewritten in terms of the similarity variables as

$$\theta_{\text{eff}} = \theta_{c,\text{org}} + \left(\frac{\rho_w}{\rho_e}\right)^{1/2}\left(\frac{\mu_w}{\rho_e U_e x}\right)^{1/2} \times \left[-\left(\frac{3}{2}\right)^{1/2} f_w + (6)^{-1/2}\int_0^\infty \left(\frac{\rho_e}{\rho} - \frac{u}{U_e}\right) d\eta\right]$$

where

$$f_w = -\rho_w V_w \left(\frac{2x}{3\rho_w \mu_w U_e}\right)^{1/2} \qquad \eta = \left(\frac{3U_e}{2\rho_w \mu_w x}\right)^{1/2} \int_0 \rho dy$$

and the resulting local pressure may then be obtained by employing the tangent-cone method. Of course, the rigorous procedure involves iterating to a final pressure distribution. However, for the cases analyzed in this analysis, the use of the original conical flow to compute the pressure interaction was sufficient. The induced pressure and pressure gradient had an insignificant effect on the slope, $d\delta^*/dx$, and on $\rho_w V_w/\rho_e U_e$.

Figure 2 illustrates induced pressure distributions on an 8° cone. Also of interest are the boundary-layer thickness and boundary-layer displacement thickness. Resulting values of these parameters are given in Table 1 and apply to the 1-ft cone station.

Table 1 Boundary-layer thickness and displacement thickness

Freestream conditions V_∞, fps	Z_∞, ft	Injected conditions	δ, ft	δ^*, ft
22,000	200,000	Teflon ablation	4.52×10^{-2}	3.45×10^{-2}
22,000	200,000	Forced air injection	3.81×10^{-2}	2.55×10^{-2}
22,000	200,000	Clean air, no injection	2.92×10^{-2}	1.8×10^{-2}
22,000	150,000	Teflon ablation	1.36×10^{-2}	1.06×10^{-2}
22,000	150,000	Clean air, no injection	1.05×10^{-2}	7.6×10^{-3}

Conclusions

1) There is a significant increase in the pressure with blowing as compared to the pressure interaction without blowing.

2) In general, for the case of blowing, the pressure interaction will be a function of the gas injection rate and a function of the injected gas itself.

References

[1] Probstein, R. F., "Interacting hypersonic laminar boundary layer flow over a cone," TR AF 2798/1, Div. Eng., Brown Univ., Providence, R. I. (March 1955).

[2] Mann, W. M., Jr., "Effective displacement thickness for boundary layers with surface mass transfer," AIAA J. **1**, 1181–1182 (1963).

[3] Van Tassell, W. and Pallone, A., "Similar solutions of the compressible laminar boundary-layer equations for air in equilibrium dissociation and ionization with and without air injection in the stagnation region," Avco RAD-TM-61-22 (June 1961).

Effects of Orthotropicity Orientation on Supersonic Panel Flutter

JOHN M. CALLIGEROS* AND JOHN DUGUNDJI†
Massachusetts Institute of Technology, Cambridge, Mass.

AN important structural aspect of the panel flutter problem is the effect of orthotropicity. Although generally it is felt that aligning stiffeners parallel to the airflow would give the maximum increase in the flutter boundary, it might be possible that some other angular orientation of the stiffeners would give a greater increase. Accordingly, this problem has been investigated for flat, rectangular, simply supported panels in a supersonic flow. This note is based on work reported in greater detail in Ref. 1 and is an extension of the basic problem of Hedgepeth.[2]

Consider the panel of Fig. 1. Using small deflection thin plate theory, the total potential energy π is given by[3]

$$\pi = \frac{1}{2}\int_0^a \int_0^b \left[D_{11}\left(\frac{\partial^2 w}{\partial x^2}\right)^2 + 2D_{12}\frac{\partial^2 w}{\partial x^2}\frac{\partial^2 w}{\partial y^2} + D_{22}\left(\frac{\partial^2 w}{\partial y^2}\right)^2 + 4D_{33}\left(\frac{\partial^2 w}{\partial x \partial y}\right)^2 + 4\frac{\partial^2 w}{\partial x \partial y} \times \left(D_{13}\frac{\partial^2 w}{\partial x^2} + D_{23}\frac{\partial^2 w}{\partial y^2}\right) - 2pw\right] dxdy \quad (1)$$

Received July 8, 1963. This research was supported by the Air Force Office of Scientific Research under Contract AF 49(638)-219.

* Senior Research Engineer, Aeroelastic and Structures Research Laboratory, Department of Aeronautics and Astronautics. Member AIAA.

† Associate Professor of Aeronautics and Astronautics. Member AIAA.

The rigidities D_{ij} are given by

$$D_{11} = D_{11}' \cos^4\phi + D_{22}' \sin^4\phi + 2(D_{12}' + 2D_{33}') \cos^2\phi \sin^2\phi$$

$$D_{12} = (D_{11}' + D_{22}' - 4D_{33}') \cos^2\phi \sin^2\phi + D_{12}'(\cos^4\phi + \sin^4\phi)$$

$$D_{22} = D_{22}' \cos^4\phi + D_{11}' \sin^4\phi + 2(D_{12}' + 2D_{33}') \cos^2\phi \sin^2\phi \quad (2)$$

$$D_{13} = [D_{22}' \sin^2\phi - D_{11}' \cos^2\phi + (D_{12}' + 2D_{33}')(\cos^2\phi - \sin^2\phi)] \cos\phi \sin\phi$$

$$D_{23} = [D_{22}' \cos^2\phi - D_{11}' \sin^2\phi - (D_{12}' + 2D_{33}')(\cos^2\phi - \sin^2\phi)] \cos\phi \sin\phi$$

$$D_{33} = (D_{11}' + D_{22}' - 2D_{12}') \cos^2\phi \sin^2\phi + D_{33}'(\cos^2\phi - \sin^2\phi)^2$$

where the principal elastic axes x'-y' are rotated an angle ϕ with respect to the geometric panel axes x-y as shown in Fig. 1. When $\phi = 0°$ or $90°$, then $D_{13} = D_{23} = 0$, thereby reducing to the classical orthotropic plate case.

Substituting the assumed deflection shape,

$$w(x,y,t) = \sum_m \sum_n C_{mn} \sin\frac{m\pi x}{a} \sin\frac{n\pi y}{b} e^{i\omega t} \quad (3)$$

which satisfies the displacement boundary conditions, applying $\delta\pi = 0$, and then substituting the following for the lateral load into Eq. (1),

$$p(x,y,t) = -\frac{\rho_A U}{M}\left(U\frac{\partial w}{\partial x} + \frac{\partial w}{\partial t}\right) - B\frac{\partial w}{\partial t} - \gamma\frac{\partial^2 w}{\partial t^2} \quad (4)$$

the following equations for flutter are obtained:

$$\left[m^4\frac{D_{11}}{D_{11}'} + 2\left(\frac{a}{b}\right)^2\frac{D_{xy}}{D_{11}'}(mn)^2 + \left(\frac{a}{b}\right)^4\frac{D_{22}}{D_{11}'}n^4 - Z\right]C_{mn} - \frac{\lambda}{\pi^3}\sum_r\sum_s C_{rs}L_{mn,rs} - 2\sum_r\sum_s C_{rs} \times \left[\left(\frac{a}{b}\right)\frac{D_{13}}{D_{11}'}(m^2 + r^2) + \left(\frac{a}{b}\right)^3\frac{D_{23}}{D_{11}'}(n^2 + s^2)\right]P_{mn,rs} = 0$$

$$(m,n,r,s = 1,2,3, \ldots) \quad (5)$$

where

$$Z = \left(\frac{\omega}{\omega_0}\right)^2 - ig_T\left(\frac{\omega}{\omega_0}\right) \qquad \omega_0 = \left(\frac{\pi^4 D_{11}'}{\gamma a^4}\right)^{1/2} \quad (6)$$

$$g_T = g_A + 2\zeta_i\frac{\omega_i}{\omega_0} \qquad g_A = \frac{0.351(1-\nu^2)^{1/2}}{[(D_{11}'/D_s)(t_E/t_s)]^{1/2}}\frac{\rho_A}{\rho_M}\frac{c_A}{c_M}\left(\frac{a}{t_s}\right)^2$$

$$\zeta_i = \frac{B}{2\gamma\omega_i} \qquad D_{xy} = D_{12} + 2D_{33} \qquad \lambda = \frac{\rho_A U^2 a^3}{MD_{11}'}$$

and where $L_{mn,rs} = 4mr/\pi(r^2 - m^2)$ if $m \pm r$ is odd and $n = s$, otherwise $L_{mn,rs} = 0$; and $P_{mn,rs} = 16\,mnrs/\pi^2(r^2 - m^2)(s^2 - n^2)$ if $m \pm r$ and $n \pm s$ are odd, otherwise $P_{mn,rs} = 0$. In the forementioned, g_T is the sum of aerodynamic and structural damping; ω_i is the free vibration frequency of the jth mode; ζ_i is the corresponding critical damping ratio; $D_s = Et_s^3/12(1 - \nu^2)$ is the bending stiffness of the basic unstiffened skin; ρ_A and ρ_M are the densities of air and panel material, respectively; c_A and c_M are the corresponding velocities of sound; γ is the panel mass per unit area; and $t_E = t_S[1 + (b_w/b_y)(t_w/t_s)]$. Aerodynamic piston theory and structural damping of the equivalent viscous type have been used.

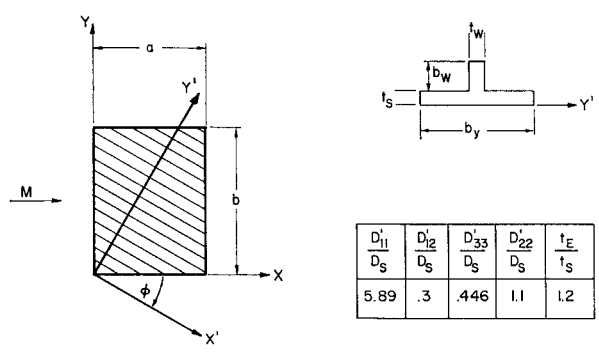

$\frac{D_{11}'}{D_s}$	$\frac{D_{12}'}{D_s}$	$\frac{D_{33}'}{D_s}$	$\frac{D_{22}'}{D_s}$	$\frac{t_E}{t_s}$
5.89	.3	.446	1.1	1.2

Fig. 1 Geometry and properties of panel.

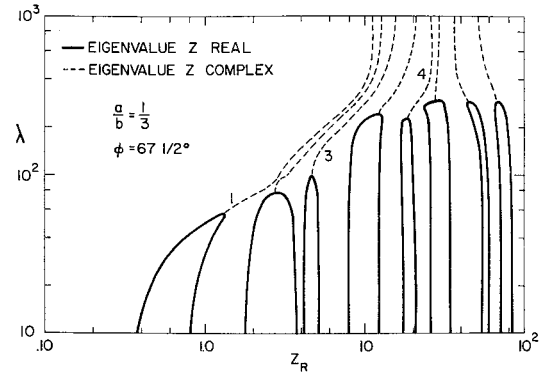

Fig. 2 Frequency coalescence plot.

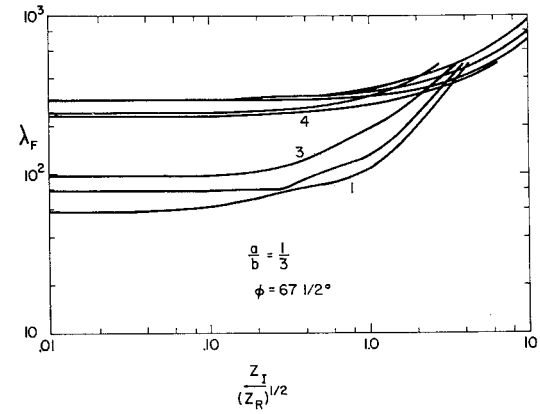

Fig. 3 Effect of damping on flutter boundary.

Undamped flutter boundaries may be obtained by the method of frequency coalescence.[2] The effect of damping may be investigated by Movchan's method,[4] which yields the following equation determining the flutter boundary:

$$Z_I/(Z_R)^{1/2} = g_A + 2\zeta_j(\omega_j/\omega_0) = g_T \quad (7)$$

where Z_I and Z_R are the real and imaginary components of the eigenvalue Z of Eq. (5). A 16-mode solution using the first four streamwise and spanwise deflection modes was obtained for the example panel of Fig. 1. A typical frequency coalescence plot and damping plot are presented in Figs. 2 and 3, respectively. It can be seen that the effect of damping (Fig. 3) is to raise the flutter boundary and to transfer coalescence from lower modes to higher modes. The effect of rotating the stiffeners is to lower the flutter boundary considerably for $a/b = 1$ (Fig. 4). It also is shown in Fig. 4 that the presence of slight damping raises significantly the flutter points resulting from "weak coalescences." For $a/b = 3$, the flutter boundary is raised, however, for some values of ϕ (Fig. 5). This may be attributed to the "membrane-like" behavior of the panel resulting from the dominance of the $2(a/b)^2D_{xy}/D_{11}'(mn)^2$ term over the bending terms of Eq. (5) at high a/b and when $\phi \approx 45°$. It appears then that aligning the stiffeners parallel to the flow ($\phi = 0$) is not necessarily the preferred orientation. Other

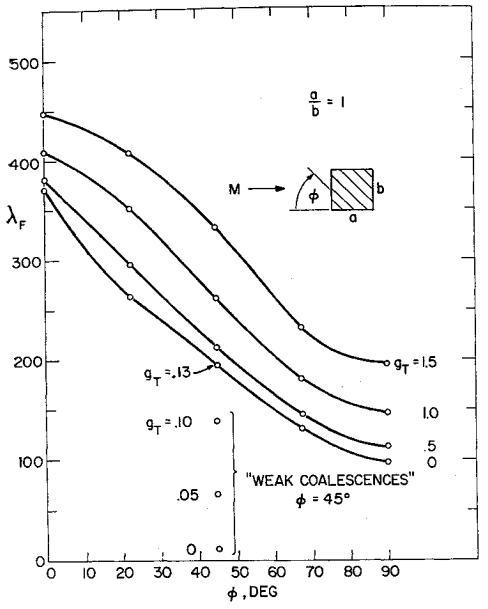

Fig. 4 Effect of angle of orthotropicity on flutter boundary.

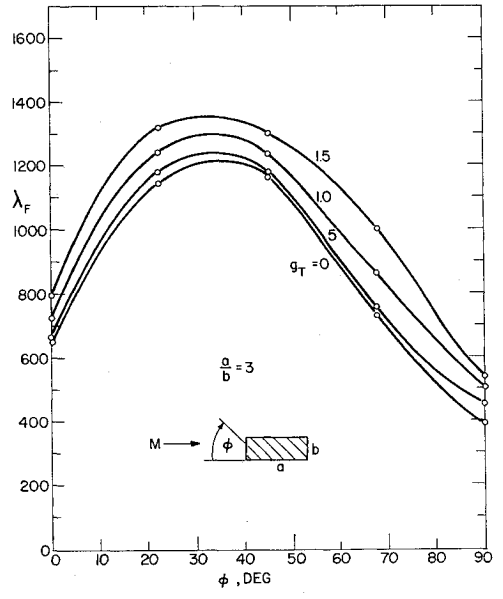

Fig. 5 Effect of angle of orthotropicity on flutter boundary.

angles may be preferred, depending primarily on a/b, amount of damping, and amount of orthotropicity present.

This investigation has limitations at high a/b. A more refined aerodynamic surface theory should be used there, because of low aspect ratio effects. Secondly, more deflection modes should be used to improve convergence because of the "membrane-like" behavior at high a/b. Qualitative trends, however, may still be revealed.

References

[1] Calligeros, J. M. and Dugundji, J., "Supersonic flutter of rectangular orthotropic panels with arbitrary orientation of orthotropicity," TR 74-5, Mass. Inst. Tech. Aeroelastic and Structures Res. Lab. (June 1963).

[2] Hedgepeth, J. M., "Flutter of rectangular simply supported panels at high supersonic speeds," J. Aeronaut. Sci. 24, 563–573 (1957).

[3] Hearmon, R. F. S., *An Introduction to Applied Anisotropic Elasticity* (Oxford University Press, London, 1961), Chap. VII, p. 94.

[4] Movchan, A. A., "On the stability of a panel moving in a gas," NASA RE 11-21-58W (1959).

Rapid Discharge of a Gas from a Cylindrical Vessel through a Nozzle

R. C. Progelhof* and J. A. Owczarek†
Lehigh University, Bethlehem, Pa.

Nomenclature

a = speed of sound
A = cross-sectional area
d = diameter of nozzle throat
L = length of cylindrical vessel
p = pressure
t = time
u = magnitude of the flow velocity
x = distance
δ^* = boundary-layer displacement thickness
γ = ratio of specific heats

Subscripts

0 = initial conditions
e = exit of nozzle
f = minimum cross-sectional area of flow stream
v = vessel

Introduction

THIS note is a continuation of the investigation on the rapid discharge of a gas from a cylindrical vessel made by the authors.[6] The constrictive devices used in these experiments were standard American Society of Mechanical Engineers long-radius flow nozzles with β ratios of approximately 0.25, 0.50, and 0.66. The experimental equipment and technique are identical to those of the previous investigation on the discharge with orifice constrictions. Figure 1 is a comparison of three oscilloscope traces for the same pressure ratio but with different nozzles. It shows how sensitive the variation of pressure with time in the vessel is to the exit area of the nozzle.

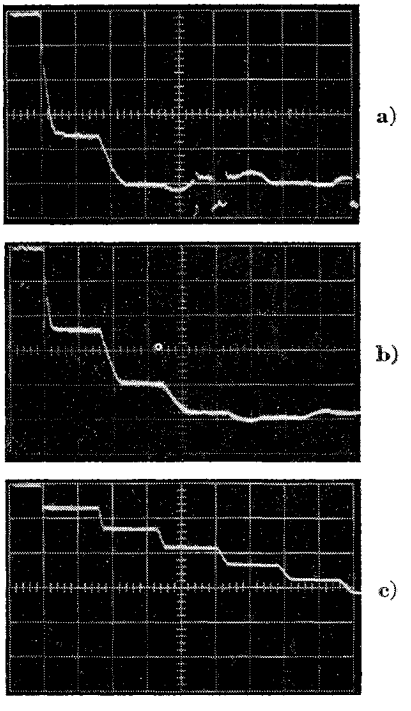

Fig. 1 Pressure record at the sealed end of the vessel, X/L = 0, for the same initial pressure, 30 psia, and oscilloscope settings with nozzle β ratios of a) 0.66, b) 0.50, and c) 0.25.

Received July 10, 1963.

* Assistant Professor, Department of Mechanical Engineering.
† Associate Professor, Department of Mechanical Engineering.